Engineered Science

RESEARCH PAPER View Article Online

Spray Pyrolytic Deposition of Zirconium Oxide Thin Films: Influence of Concentration on Structural and Optical Properties

Mangesh Waghmare,[1,2] Pratik Sonone,[1] Prashant Patil,[3] Vishal Kadam,[2] Habib Pathan[2] and Ashok Ubale[1*]

Zirconium oxide (ZrO_2) thin films were deposited by spray pyrolysis technique using precursor solution of zirconyl chloride octahydrate ($ZrOCl_2.8H_2O$) on glass substrate at 450 °C. The effects of concentration of precursor solution on the structural and optical properties of ZrO_2 films were investigated. The films were characterized by X- ray diffraction (XRD), Scanning electron microscopy (SEM), Energy-dispersive X-ray spectroscopy (EDX), Transmission electron microscopy (TEM), UV-vis analysis and Fourier transform infrared (FT-IR) spectroscopy. The films were amorphous in nature at 0.025 M concentration and it was observed that crystallinity increases with increase in concentration of precursor solution. The crystalline films exhibited cubic zirconium oxide (*c*-ZrO_2) phase. The surface morphology of the films was strongly influenced by the concentration of the precursor solution. The EDX study confirmed the existence of Zr and O. The TEM images showed nanosized as well as agglomerated ZrO_2 particles with the average particle size < 20 nm. The well-crystallized cubic phase of the films was further enlightened by selected area electron diffraction patterns. The UV-vis study showed that the optical band gap values were decreased with decrease in concentration of precursor solution. The formation of zirconium oxide was further confirmed by FT-IR spectroscopy.

Keywords: Nanostructured thin films; Zirconium oxide; Cubic zirconia; Spray pyrolysis

Received 3 October 2018**, Accepted** 15 November 2018

DOI: 10.30919/es8d622

1. Introduction

Zirconium oxide thin films have acquired considerable attention in the variety of applications such as protective coatings, insulating dielectric layers, catalysts, sensors and fuel cells as the properties of the films are found to be dependent on the growth conditions and methods of synthesis. Many efforts have been put in the development of low cost techniques which can offer the desired optical and structural characteristics of the material. ZrO_2 has been rigorously studied from the past few decades because of its distinct properties like high chemical inertness, low thermal conductivity, high dielectric constant, high transparency in the visible and near infrared region and high refractive index.[1, 2] Several methods have been employed for the deposition of ZrO_2 thin films which include sputtering,[3] spin coating,[4] sol–gel,[5] radio-frequency sputtering,[6] pulsed laser deposition,[7] metal–organic chemical vapour deposition[8] and spray pyrolysis.[9] However, spray pyrolysis has become one of the preferred methods for the deposition of thin transparent oxide layers due to some of its distinct advantages such as lower crystallization temperature, homogeneity, simplicity, excellent compositional control and cost effectiveness.

Ruiz *et al*.[10] have obtained zirconia films by spray pyrolysis technique and investigated the effects of composition of substrate (carbon steel, stainless steel, alumina and borosilicate glass), time (1 and 2 h), temperature (450 °C and 650 °C), and carrier gas (Ar, N, He and air) on characteristics of the films. Stelzer and Schoonman[11] have deposited zirconium oxide films by spray pyrolysis using Zr-acetylacetonate [$(Zr(C_5H_5O_2)_4$] as precursor. Peshev *et al*.[12] have used oxalic acid and zirconyl chloride octahydrate to prepare a precursor solution. The study showed that the spray pyrolytic deposited films on silica substrate were amorphous in nature. On heat treatment, cubic zirconia phase was detected in the films at temperatures T = 500-700 °C. Both cubic and monoclinic phases were detected as temeperature rises from 700 - 1000 °C. The *c*-ZrO_2 content decreases with increase in temperature. Ortiz *et al*.[13] have deposited zirconium oxide films onto fused quartz and silicon in the temperature range of 300 C to 575 °C by the pyrosol process using precursor solution of zirconium acetylacetonate. The films were found to be amorphous in nature below 425 °C. The cubic crystalline phase was observed for short deposition times and higher temperatures. The films showed monoclinic crystalline phase for long deposition times. Ramos-Guerra *et al*.[14] have studied structural and photoluminescence properties of un-doped and ZrO_2 films doped with Tb^{3+} and Eu^{3+} ions by ultrasonic spray pyrolysis technique. The XRD study demonstrated the polycrystalline nature and the existence of tetragonal metastable phase of the films. They revealed that the deposition temperature decides the surface morphological characteristics of the films. The photoluminescence analyses of the films presented a broad emission peak associated with radiative transition

[1]*Nanostructured Thin Film Materials Laboratory, Department of Physics,Govt. Vidarbha Institute of Science and Humanities, Amravati - 444604, India*
[2]*Advanced Physics Laboratory, Department of Physics, Savitribai Phule Pune University, Pune - 411007, India*
[3]*Sinhgad Institute of Technology, Lonavala - 410401, India*
***E-mail:** ashokuu@yahoo.com*

within ZrO_2 matrix at 440 nm as well as characteristic emission peaks associated with Eu^{3+} and Tb^{3+} ions. Also, it was noticed that the intensity of the photoluminescence emission increases with increase in deposition temperature. Jothibas *et al*.[15] have deposited ZrO_2 thin films at various substrate temperatures in the range 275-475 °C. The XRD study demonstrated that the crystallite size of the films increases with increase in substrate temperature. Further, the study confirmed the tetragonal phase of ZrO_2. The UV-vis spectroscopic analyses revealed that with increase in the substrate temperature, the band gap value of the film increases.

Depending on temperature and atmospheric pressure conditions, ZrO_2 exists in three polymorphs: monoclinic (*m*-ZrO_2) phase which the stable phase from room temperature up to 1100 °C, tetragonal (*t*-ZrO_2) phase in the range 1100 °C to 2300 °C and cubic (*c*-ZrO_2) phase above 2300 °C.[12] However, at low temperatures, the existence of both tetragonal and cubic metastable phases has been reported by number of research groups. These polymorphic forms depend upon dopants, the presence of impurities, the particle size, the preparatory conditions and precursors.

The present study reports the deposition of ZrO_2 thin films on glass substrates by spray pyrolysis technique. The effects of concentration of precursor solution on the structural and optical properties of ZrO_2 films were investigated.

2. Experimental section

The materials for thin film deposition were zirconyl chloride octahydrate ($ZrOCl_2 \cdot 8H_2O$) and distilled water by SRL, Mumbai. The ZrO_2 films were deposited using $ZrOCl_2 \cdot 8H_2O$ dissolved in distilled water. The precursors were kept ready by varying molarity of solution, thus, four solutions, labeled as C1, C2, C3 and C4 (see Table 1). The flow rate of the carrier gas was 35 L/min. The distance between the

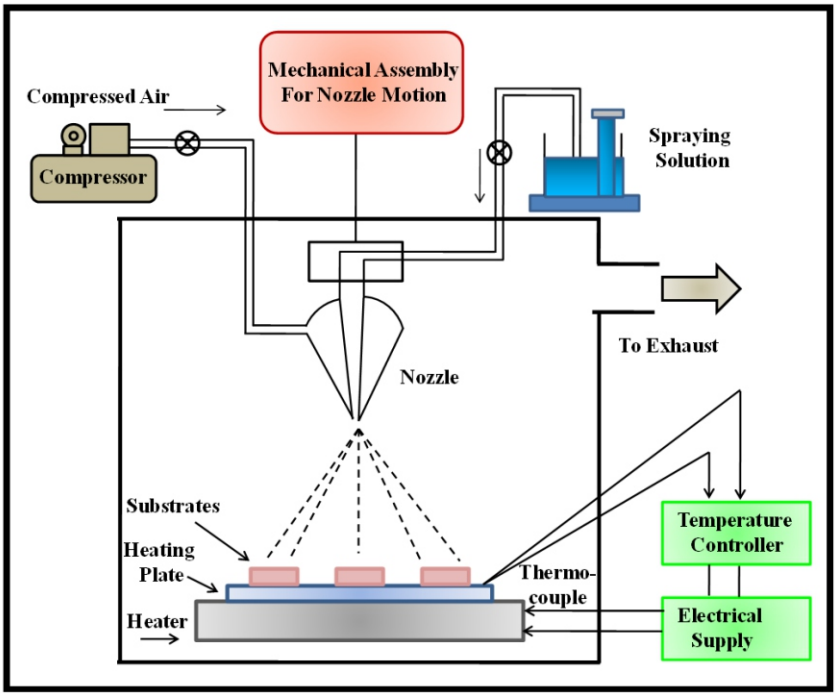

Fig. 1 Schematic of spray pyrolysis technique.

Table 1 Preparatory conditions for the deposition of ZrO_2 thin films (different concentration of precursor solution).

Sample	Concentration of Solution	Temperature (°C)	Spray Time (min)	Spray Rate (ml/min)	Flow Rate (L/min)
C1	0.025 M	450	2	7.5	35
C2	0.05 M	450	2	7.5	35
C3	0.075 M	450	2	7.5	35
C4	0.1 M	450	2	7.5	35

substrate and nozzle was 25 cm. The compressed air was used as a carrier gas to spray the precursors at the rate of 7.5 ml/min. The tin bath temperature was maintained as 450 °C and the glass substrates were kept on it. Fig. 1 shows the schematic of spray pyrolysis technique.

The crystal structure and crystallinity of the deposited films were investigated by X-ray diffraction (XRD). The patterns were obtained on Rigaku "D/B max-2400" (λ = 1.54 Å) X-ray diffractometer. The surface morphology of the deposited films was observed by scanning electron microscopy (SEM, JEOL-JSM 6360-A). The compositions of the deposited metal oxide films were analyzed by scanning electron microscope (SEM, JEOL-JSM 6360-A) equipped with an energy dispersive X-ray (EDX) detector. Transmission electron microscopic (TEM) investigations were conducted on PHILIPS CM 200 (Operating voltage: 200 kv, Resolution: 2.4 Å) microscope. The optical properties of the ZrO_2 thin films were studied in the wavelength region of 200–800 nm using UV–vis spectrometer (JascoV-670). The FT-IR spectra of the ZrO_2 thin films were recorded in the range from 400 to 4000 cm^{-1} in transmittance mode using FT-IR-6100 type A spectrometer.

3. Results and Discussion

3.1 Structural analysis

The XRD patterns of ZrO_2 thin films deposited onto glass substrate at 450 °C at various concentrations of precursor solution are shown in Fig. 2. The XRD pattern of the as-deposited ZrO_2 film (Fig. 2*a*) shows that it is amorphous in nature which indicates that the imposing material does not have adequate concentration to produce a crystalline phase. Xiaming *et al*.[16] have reported that ZrO_2 molecules are formed during the pyrolytic reaction without intrinsic close links at the same substrate temperature. This is an amorphous phase which is very much close to cubic phase of ZrO_2. During crystallization, firstly, metastable *c*-ZrO_2 is obtained and then depending upon the preparatory conditions it gets transformed to *m*-ZrO_2 or *t*-ZrO_2. In Fig. 2*b-d*, it is seen that in case of C2 sample crystallization has begun which increases with increase in concentration. The four major peaks corresponding to (111), (200), (220) and (311) planes confirm the cubic crystal structure in case of all the ZrO_2 thin film samples.[10, 12, 14, 21] All these polycrystalline ZrO_2 films are free from impurities as no impurity peaks are observed. The positions of all the peaks are in accordance with the standard ZrO_2 data (JCPDS: 27-0997) (see Table 2). The intensity of above peaks increases with increasing concentration of solution up to 0.1 M due to the improvement in crystallinity of the films. The average crystallite size (*D*) was calculated by the Scherrer formula[17] using the full width at half maximum (FWHM) of the most intense peak for different samples,

$$D = \frac{0.9\lambda}{\beta \cos\theta} \quad (1)$$

Where, β is the FWHM in radians, λ is the wavelength used and θ is the Bragg's angle. The crystallite size of C2, C3 and C4 is 12 nm, 9 nm and 11 nm, respectively. To find the defects in the nanocrystalline ZrO_2 films, the dislocation density was calculated using the relation,[18]

$$\text{Dislocation density } (\delta) = \frac{1}{D^2} \quad (2)$$

The dislocation density was calculated for the given crystallite size. The dislocation density is high for small crystallite due to more number of interfaces in the given volume. The micro strain of the sample was also estimated using the equation,[18]

$$\text{Micro strain } (\varepsilon) = \frac{\beta \cos\theta}{4} \quad (3)$$

The micro strain, dislocation density and crystallite size for nanocrystalline ZrO_2 films are listed in Table 3.The existence of defects around the lattice could be known from the micro strain. From the observations, it can be concluded that the re-crystallization process in case of polycrystalline films leads to changes in δ and ε.[15, 19]

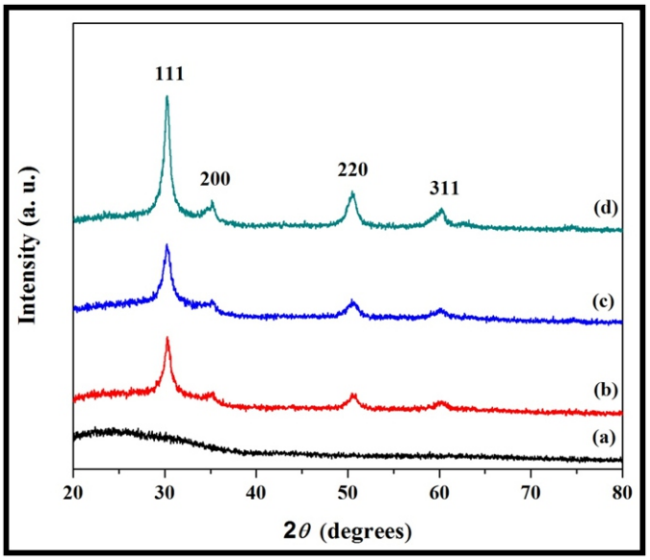

Fig. 2 Influence of concentration of precursor solution on XRD patterns of ZrO_2 thin films deposited onto glass substrate at 450 °C: (*a*) 0.025 M; (*b*) 0.05 M; (*c*) 0.075 M; (*d*) 0.1 M.

3.2 Surface morphological and elemental analysis

Fig. 3 shows SEM images of ZrO_2 films deposited at different molar concentrations. D. Perednis *et al*.[20] have reported that chlorine impurities hinder the crystallization and hence, initially, the films are amorphous in case of chlorides. For C1, a thin and transparent layer was deposited on the glass substrate. The layer was free from cracks. On the other hand, slightly larger cracks are seen in the films for C4 (0.1 M) solution (Fig. 3*d*) compared to the C1 (0.025 M), C2 (0.05 M) and C3 (0.075 M) salt solutions (Fig. 3*a-c*). With increase in the concentration of precursor solution, the particle size increases on drying. The spreading of droplets could be the deciding parameter to bring the changes in surface morphology of the films. The roughness of the films is strongly influenced by the rate at which the liquid droplets spread. As viscosity of solution increases that decreases the spreading rate of liquid droplets. In case of the droplets of C1, C2, C3 and C4 concentrated solutions, the spreading of droplets decreases due to increase in viscosity. If rapid drying process is implemented that increases the surface roughness of the films due to incomplete spreading of liquid droplets. It can be concluded that for the deposition of smooth and dense films the concentration of spraying solution should not be too high. However, in order to achieve high deposition rates, a high salt concentration is preferred. It was observed that the increase in salt concentration in the precursor solution increases the surface roughness of the deposited film. The EDX spectra show the presence of Zr and O (Fig. 4*a-c*).

The size and morphology of zirconia samples deposited at 450 °C were further explored with TEM analyses. Fig. 5*a-c* show influence of concentration of solution on TEM images of the ZrO_2 coatings. The TEM images confirm that the flakes consist of agglomerates of ZrO_2 nanoparticles with the average particle size < 20 nm. The selected area electron diffraction (SAED) pattern shows that the formed layer was composed of crystalline ZrO_2 nanoparticles (Fig. 5*d-f*). Further, the

Table 2 Comparison of observed XRD data of ZrO_2 thin films obtained after spray pyrolysis at different concentrations of precursor solution with the standard JCPDS data (JCPDS 27-0997).

Sample	Standard Values		Observed Values		h	k	l
	2θ (deg.)	d (nm)	2θ (deg.)	d (nm)			
C2	30.51	0.2929	30.22	0.2957	1	1	1
	35.19	0.2550	35.34	0.2539	2	0	0
	50.69	0.1800	50.55	0.1805	2	2	0
	60.34	0.1533	60.12	0.1539	3	1	1
C3	30.51	0.2929	30.22	0.2957	1	1	1
	35.19	0.2550	35.18	0.2550	2	0	0
	50.69	0.1800	50.55	0.1805	2	2	0
	60.34	0.1533	60.12	0.1539	3	1	1
C4	30.51	0.2929	30.22	0.2957	1	1	1
	35.19	0.2550	35.18	0.2550	2	0	0
	50.69	0.1800	50.55	0.1805	2	2	0
	60.34	0.1533	60.28	0.1535	3	1	1

Table 3 Crystallite size, dislocation density and micro strain of ZrO_2 thin films obtained at different concentrations of precursor solution.

Sample	Crystallite Size, D (nm)	Dislocation Density, δ (10^{14} m^{-1})	Micro strain, ε (10^{-4})
C2	12	69.44	29.57
C3	9	123.45	38.27
C4	11	82.64	31.27

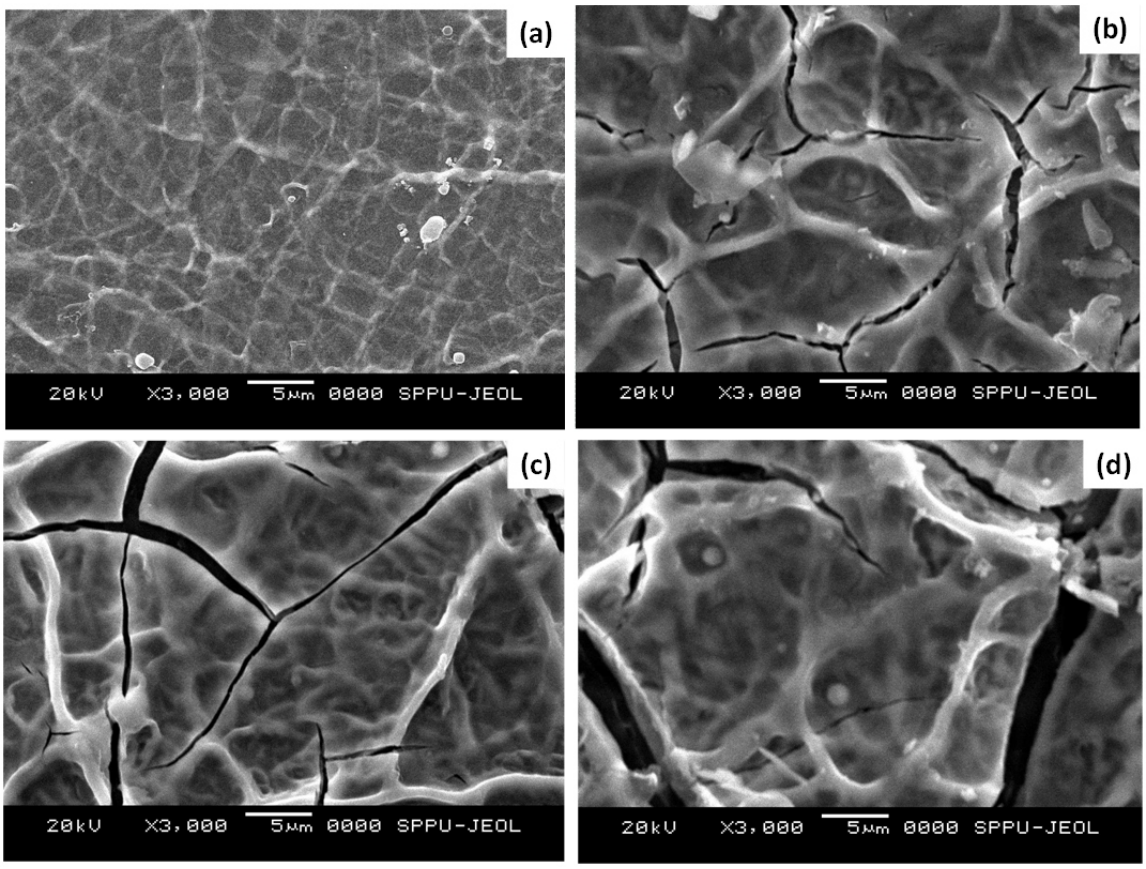

Fig. 3 Scanning electron micrographs of ZrO_2 thin films on glass substrate. Deposition condition (concentration of precursor solution): (*a*) 0.025 M; (*b*) 0.05 M; (*c*) 0.075 M; (*d*) 0.1 M.

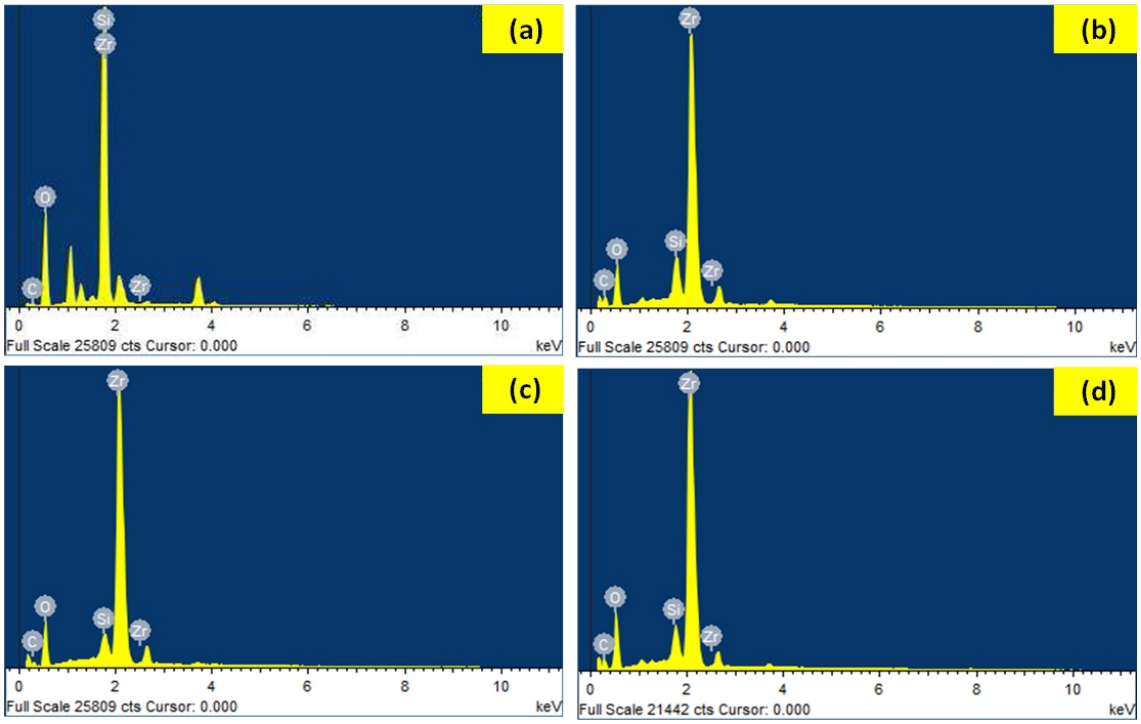

Fig. 4 EDX spectra of ZrO_2 thin films on glass substrate. Deposition condition (concentration of precursor solution): (*a*) 0.025 M; (*b*) 0.05 M; (*c*) 0.075 M; (*d*) 0.1 M.

SAED patterns give spot pattern. However, it seems it is not a single pattern, but a more complex pattern which could be caused by aggregates of nanoparticles. The d-spacing corresponding to the diffraction rings of the SAED patterns is in accordance with the cubic phase of ZrO_2 nanocrystals. The SAED patterns of the aggregates of ZrO_2 nanoparticles confirm the nanocrystallinity of the films. The concentric Debye–Scherrer rings can be indexed to the (111), (200), (220) and (311) planes and are assigned to the cubic phase. The results show that no phase transformation occurs with increase in concentration of precursor solution. The crystallite size obtained from the X-ray diffraction and TEM results are in good agreement.

3.3 UV-vis analysis

The optical absorption measurements were carried out in the wavelength region of 200-800 nm to estimate the optical band gap energy. The optical band gap (E_g) in ZrO_2 thin films was estimated using the relationship between the absorption coefficient (α) and the photon energy ($h\upsilon$) given by the equation

$$\alpha = \frac{A\,(E_g - h\upsilon)^n}{h\upsilon} \tag{4}$$

where A is a constant, α is absorption coefficient, E_g is the band gap energy, and n is equal to 2 for indirect and ½ for direct transition. Fig. 6 shows the plot of $(\alpha h\upsilon)^2$ versus $h\upsilon$ of ZrO_2 thin films deposited on glass substrate for different concentration of precursor solution. The optical band gap was determined by extrapolating the straight line portion of the plot to the energy axis for $\alpha = 0$.[21] The optical band gap values were found to be 4.18 eV (for 0.1 M concentration), 4.03 eV (for 0.075 M and 0.05 M) and 4.05 eV (for 0.025 M). It has been observed that the optical band gap deceases with decrease in concentration of precursor solution. The decrease in optical band gap of the films could be attributed to changes in structural defects, grain size and atomic distances. The improvement in crystallinity and morphology of the film decreases the optical band gap of the material with increase in concentration of precursor solution.[22, 23] The inset of Fig. 6 shows the optical absorption spectra of ZrO_2 thin films deposited on glass substrate

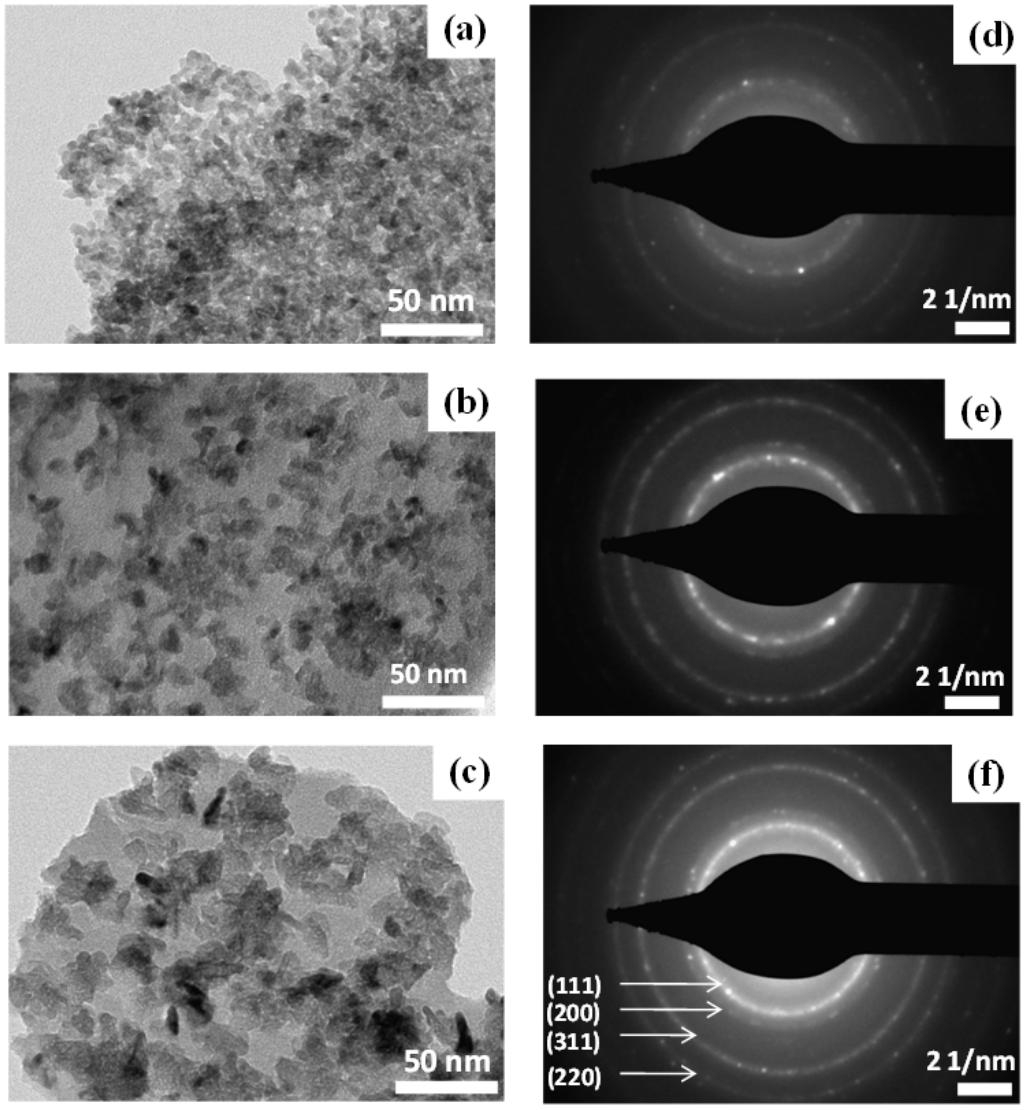

Fig. 5 TEM images of ZrO_2 thin films on glass substrate at 450 °C. Deposition condition (concentration of precursor solution): (*a*) 0.05 M; (*b*) 0.075 M; (*c*) 0.1 M. The Corresponding SAED patterns: (*d*) 0.05 M; (*e*) 0.075 M; (*f*) 0.1 M.

at different concentration of precursor solution at 450 °C. In visible region, the optical absorption spectra revealed the low absorbance characteristic feature of ZrO_2.

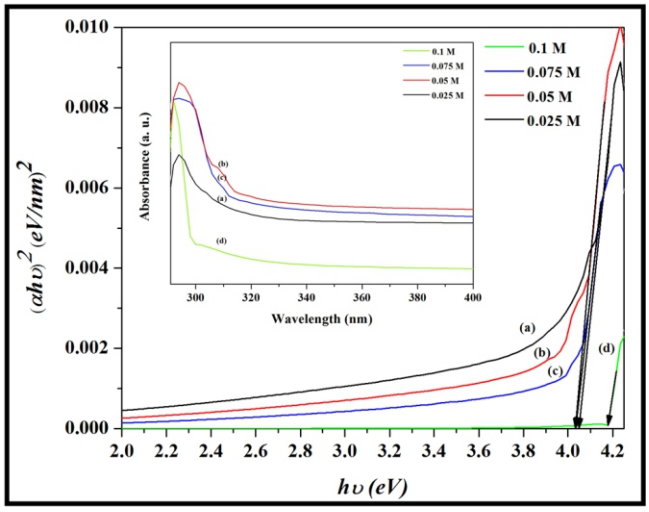

Fig. 6 Variation of $(\alpha h\upsilon)^2$ versus $h\upsilon$ of ZrO_2 thin films deposited onto glass substrate at 450 °C: (*a*) 0.025 M, (*b*) 0.05 M, (*c*) 0.075 M, (*d*) 0.1 M. The inset shows variation in absorbance with wavelength of ZrO_2 thin films: (*a*) 0.025 M, (*b*) 0.05 M, (*c*) 0.075 M, (*d*) 0.1 M.

3.4 FTIR analysis

Fig. 7 shows influence of concentration of precursor solution on the FT-IR spectra of zirconia films. The C1 film sample exhibited O-H stretching vibration in the frequency range 3406-3908 cm^{-1} (see Fig. 7*a*). This could be due to the interaction between Zr^{4+} and inner hydroxyl groups. This interaction builds superior force of attraction on the stretching vibration due to reduction in the vibrational dipole moment. Hence, in case of C2, C3 and C4 zirconia film samples the structural vibration for O-H were appeared at wave number greater than 3000 cm^{-1} (see Fig. 7*b-d* and refer Table 4). The O-H stretching vibrations were observed at 3980, 3783, 3595 and 3461 cm^{-1} in case of C2. In C3 sample, the O-H stretching vibrations were appeared at 3962, 3792, 3658 and 3587 cm^{-1} whereas at 3968, 3778, 3652 and 3601 cm^{-1} for C4.[24, 25] The vibrations appeared at 2941, 2932, 2923 and 2937 cm^{-1} for C1, C2, C3 and C4 respectively which could be ascribed to the impurities in the form of organic residues.[26] The bands appeared at 2296 cm^{-1} for C1, 2296 cm^{-1} for C2, 2306 cm^{-1} for C3 and 2358 cm^{-1} for C4 can be attributed to adsorbed CO_2 vibrations.[27] The bands observed at 1589 cm^{-1} for C1, 1598 cm^{-1} for C2, 1582 cm^{-1} for C3 and 1549 cm^{-1} for C4 could be due to the N-O asymmetric stretching vibration. For all samples, the vibration appeared at 1428 cm^{-1} could be ascribed to C-C stretching vibration.[28, 29] The C-N stretching vibrations were observed at 1024 cm^{-1} for C2, 1030 and 1091 cm^{-1} for C3 and 1021 and 1092 cm^{-1} for C4. For C1 and C2, O-H bending vibration was appeared at 899 and 944 cm^{-1} respectively.[26-29]

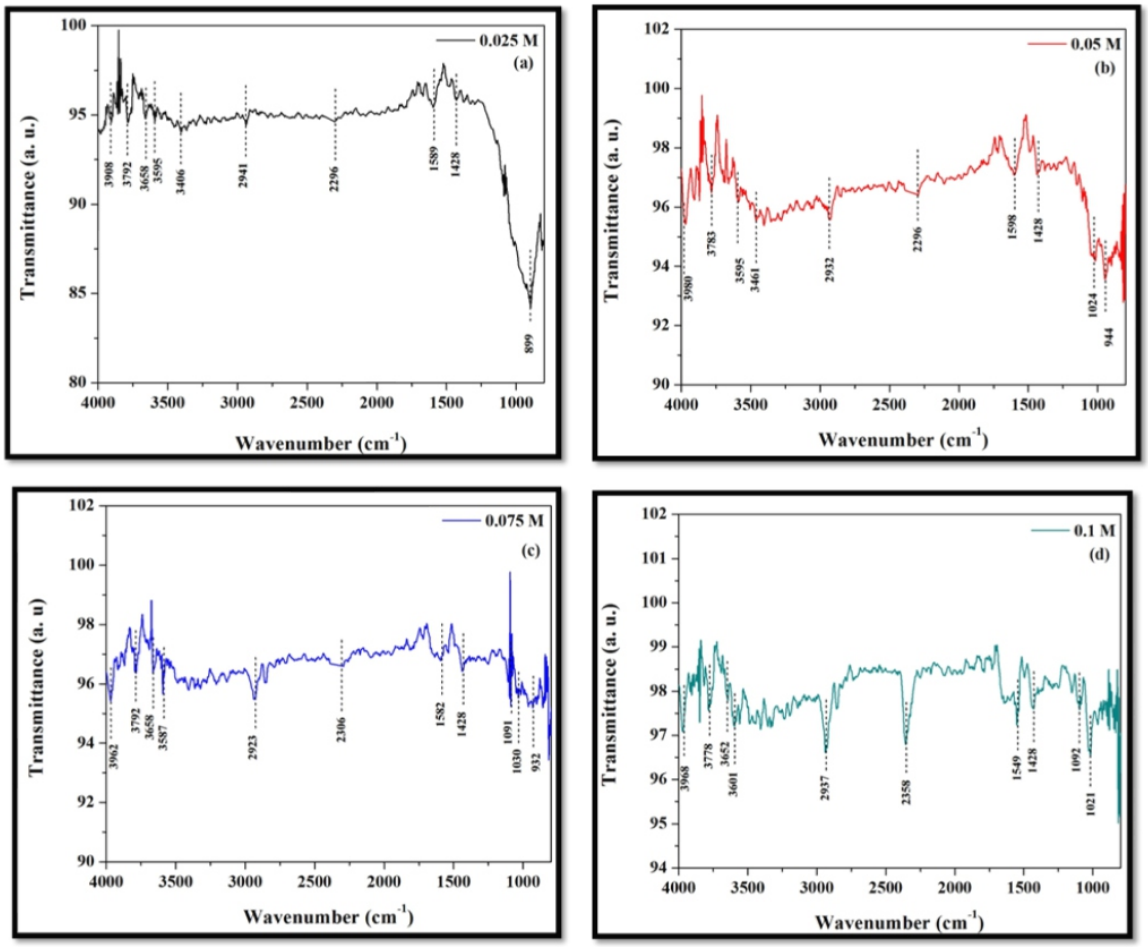

Fig. 7 FT-IR spectra of ZrO_2 thin films on glass substrate at 450 °C. Deposition condition (concentration of precursor solution): (*a*) 0.025 M; (*b*) 0.05 M; (*c*) 0.075 M; (*d*) 0.1 M.

Table 4 IR spectral frequency (cm^{-1}) of ZrO_2 films with respect to concentration of precursor solution.

Sample			
C1	**C2**	**C3**	**C4**
3908	3980	3962	3968
3792	3783	3792	3778
3658		3658	3652
3595	3595	3587	3601
3406	3461		
2941	2932	2923	2937
2296	2296	2306	2358
1589	1598	1582	1549
1428	1428	1428	1428
		1091	1092
	1024	1030	
899	944	932	

4. Conclusions

A precursor solution of zirconyl chloride octahydrate ($ZrOCl_2 \cdot 8H_2O$) can be used to deposit zirconium oxide films by spray pyrolysis technique. The influence of concentration of precursor solution on the structural and optical properties of ZrO_2 films were investigated by XRD, SEM, EDX, TEM, UV- vis and FT-IR techniques. XRD analyses demonstrated that the films prepared at lower concentration (0.025 M) were found to be in amorphous phase. The increase in concentration from 0.05 M to 0.1 M of precursor solution increases the crystallinity of the films. Only cubic zirconia (*c*-ZrO_2) phase was indentified in all the crystalline film samples at substrate temperature of 450 °C. TEM studies showed that the average particle size in all film samples was < 20 nm. The SAED patterns showed that films composed of crystalline cubic ZrO_2 nanocrystals. The optical band gap values of the deposited films were increased with increase in concentration of precursor solution. The formation of ZrO_2 was further confirmed by FT-IR studies.

Conflicts of interest

There are no conflicts to declare

Acknowledgements

Authors are thankful to Board of College and University Development (BCUD), Savitribai Phule Pune University, Pune for financial support under the project.

References

1. D. H. Kuo and C. H. Chien, *Thin Solid Films*, 2003, **429**, 40-45.
2. S. Zhao, F. Ma, K. W. Xu and H. F. Liang, *J. Alloys Compd.*, 2008, **453**, 453-457.
3. A. P. Huang and P. K. Chu, *Mater. Sci. Eng. B*, 2005, **121**, 244-247.
4. M. Asilturk, E. Burunkaya, F. Sayılkan, N. Kiraz and E. Arpaç, *J. Non-Cryst. Solids*, 2011, **357**, 206-210.
5. K. Joy, I. J. Berlin, P. B. Nair, J. S. Lakshmi, G. P. Daniel and P. V.

Thomas, *J. Phys. Chem. Solids*, 2011, **72**, 673-677.
6. H. Tomaszewski, J. Haemers, J. Denul, N. De Roo and R. De Gryse, *Thin Solid Films*, 1996, **287**, 104-109.
7. J. C. Delgado, F. Sánchez, R. Aguiar, Y. Maniette, C. Ferrater and M. Varela, *Appl. Phys. Lett.*, 1996, **68**, 1048-1050.
8. Z. Chen, N. Prud'homme, B. Wang and V. Ji, *Surf. Coat. Technol.*, 2011, **206**, 405-410.
9. D. Nguyen, M. van Roode and S. Johar, *Thin solid films*, 1986, **135**, L19-L21.
10. H. Ruiz, H. Vesteghem, A. R. Di Giampaolo and J. Lira, *Surf. Coat. Technol.*, 1997, **89**, 77-81.
11. N. H. J. Stelzer and J. Schoonman, *J. Mater. Synth. Process*, 1996, **4**, 429-438.
12. P. Peshev, I. Stambolova, S. Vassilev, P. Stefanov, V. Blaskov, K. Starbova and N. Starbov, *Mater. Sci. Eng. B*, 2003, **97**, 106-110.
13. A. Ortiz, J. C. Alonso and E. Haro-Poniatowski, *J. Electron. Mater.*, 2005, **34**, 150-155.
14. A. I. Ramos-Guerra, J. Guzman-Mendoza, M. García-Hipólito, O. Alvarez-Fregoso and C. Falcony, *Ceram. Int.*, 2015, **41**, 11279-11286.
15. M. Jothibas, C. Manoharan, S. J. Jeyakumar, P. Praveen and I. J. Panneerdoss, *J. Mater. Sci. - Mater. Electron.*, 2016, **27**, 5851-5859.
16. D. Xiaming, L. Qingfeng and T. Yuying, *J. Am. Ceram. Soc.*, 1993, **76**, 760-762.
17. B. D. Cullity, *Elements of X-ray Diffraction*, *Addison-Wesley Publishing Company, Inc., London*, 1978, **99**.
18. A. U. Ubale and M. R. Belkhedkar, *J. Mater. Sci. Technol.*, 2015, **31**, 1-9.
19. M. Jothibas, C. Manoharan, S. Ramalingam, S. Dhanapandian, S. J. Jeyakumar and M. Bououdina, *J. Mol. Struct.*, 2013, **1049**, 239-249.
20. D. Perednis, O. Wilhelm, S. E. Pratsinis and L. J. Gauckler, *Thin solid films*, 2005, **474**, 84-95.
21. B. Karunagaran, R. T. Rajendra Kumar, C. Viswanathan, D. Mangalaraj, S. K. Narayandass and G. Mohan Rao, *Cryst. Res. Technol.*, 2003, **38**, 773-778.
22. Y. Akaltun, M. A. Yıldırım, A. Ateş and M. Yıldırım, *Opt. Commun.*, 2011, **284**, 2307-2311.
23. S. Visalakshi, R. Kannan, S. Valanarasu, H. S. Kim, A. Kathalingam and R. Chandramohan, *Appl. Phys. A*, 2015, **120**, 1105-1111.
24. D. Sarkar, D. Mohapatra, S. Ray, S. Bhattacharyya, S. Adak and N. Mitra, *Ceram. Int.*, 2007, **33**, 1275-1282.
25. G.Y. Guo and Y. L. Chen, *J. Mater. Chem.*, 2001, **11**, 1283–1287.
26. A. J. Maira, K. L. Yeung, J. Soria, J. M. Coronado, C. Belver, C. Y. Lee and V. Augugliaro, *Appl. Catal. B-Environ.*, 2001, **29**, 327-336.
27. M. A. Waghmare, K. S. Pawar, H. M. Pathan and A. U. Ubale, Mater. Sci. Semicond. Process., 2017, **72**, 122-127.
28. C. M. Phillippi and K. S. Mazdiyasni, *J. Am. Ceram. Soc.*, 1971, **54**, 254-258.
29. S. Chen, Y. Yin, D. Wang, Y. Liu and X. Wang, *J. Cryst. Growth*, 2005, **282**, 498-505.